A Journal of the Gesellschaft Deutscher Chemiker

Angewandte International Edition GDCh Chemie

www.angewandte.org

Accepted Article

Title: Isolable Tetragold(0) Clusters with Polarity-Tunable exo-Au–Au Bond via Intramolecular σ-Aromatization

Authors: Jiaxin Chen, Lu Huang, Lifang Wu, Yichi Zhang, Rong Zhang, Yinhuan Li, Yunqing Zhao, Liliang Wang, Dewei Feng, Mitsuo Kira, Zhenyang Lin, and Zhifang Li

To be cited as: *Angew. Chem. Int. Ed.* **2023**, e202311230

Link to VoR: https://doi.org/10.1002/anie.202311230

WILEY VCH

10.1002/anie.202311230

WILEY VCH

COMMUNICATION

Isolable Tetragold(0) Clusters with Polarity-Tunable *exo*-Au–Au Bond via Intramolecular σ-Aromatization

Jiaxin Chen,†[a,b] Lu Huang,†[a] Lifang Wu,[a] Yichi Zhang, [b] Rong Zhang,[a] Yinhuan Li,[a] Yunqing Zhao,[a] Liliang Wang,*[a] Dewei Feng,[a] Mitsuo Kira,[a] Zhenyang Lin,*[b] and Zhifang Li*[a]

[a] J. Chen, L. Huang, L. Wu, R. Zhang, Y. Li, Y. Zhao, Prof. Dr. L. Wang, D. Feng, Prof. Dr. M. Kira, Prof. Dr. Z. Li
College of Material Chemistry and Chemical Engineering, Key Laboratory of Organosilicon Chemistry and Material Technology, Ministry of Education, Key Laboratory of Organosilicon Material Technology of Zhejiang Province, Hangzhou Normal University
Hangzhou (China)
E-mail: lwang@hznu.edu.cn; zhifanglee@hznu.edu.cn

[b] J. Chen, Y Zhang, Prof. Dr. Z. Lin
Department of Chemistry, The Hong Kong University of Science & Technology
Clear Water Bay, Kowloon, Hong Kong (China)
E-mail: chzlin@ust.hk

† These authors contributed equally to this work.

Supporting information for this article is given via a link at the end of the document.

Abstract: Intramolecular π-aromatization is a trait of many organic compounds that enhances the stability of their structures and polarizes related C–C π bonds. In contrast, rare study is focused on this phenomenon in metal clusters. Many existing homometallic clusters exhibit aromaticity, often characterized by nonpolar metal-metal bonds and a high degree of symmetry. However, synthesizing low-symmetric homometallic clusters with high-polar metal-metal bonds is challenging due to their limited thermodynamic stability. Herein, we report a facile strategy for the synthesis of $[Au(\mu_2\text{-}ER_2)]_3$–$AuPMe_3$ (E = Ge, Sn; R_2 = 1,1,4,4-tetrakis(trimethylsilyl)butane-1,4-diyl) clusters and reveal a novel stabilization mode, intramolecular σ-aromatization. Our electronic structure analyses show that these low-symmetric clusters possess a ten-electron σ-aromatic system, which is achieved via intramolecular σ-aromatization. Moreover, the strength of σ-aromaticity gives rise to a polarity-tunable *exo*-Au–Au bond.

In 1825, Faraday's discovery of benzene paved the foundation for Hofmann to introduce the concept of aromaticity in 1856. [1] Since then, aromaticity has expanded to include a wide range of compounds, ranging from organic to inorganic, with descriptors evolving into four criteria: geometric, energetic, magnetic, and electronic. Nowadays, new types of aromaticity have emerged, including heteroaromaticity, Möbius aromaticity, three-dimensional aromaticity, and excited state aromaticity.[2] In recent decades, various planar homometallic clusters have been synthesized and have often been discovered with aromaticity and high symmetry. For example, Wang and co-workers invoked σ-aromaticity to explain the stability of the square planar $[Al_4]^{2-}$ cluster, which was later demonstrated by Islas *et al.* as doubly aromatic with both σ and π electrons being delocalized.[3] Afterwards, the concept of σ-aromaticity was extended to the designing and synthesis of other triangular clusters subsequently, such as $[(LAu)_3]^+$ (L = N-heterocyclic carbene and *cyclic*-(alkyl)-(amino) carbenes),[4] $[(R_2EAu)_3]^-$ (E = Si, Ge, and Sn; R_2=1,1,4,4-tetrakis(trimethylsilyl)butane-1,4-diyl),[5] $[Zn_3Cp^*_3]^+$ (Cp* = η-C_5Me_5),[6] anionic metal $Ta_3O_3^-$,[7] and $[Th(C_8H_8)Cl_2]_3^{2-}$ cluster.[8] As above, exisiting homometallic clusters with aromaticity usually consist of nonpolar metal-metal bonds due to their stable aromatic non-polarized Lewis structures, restricting the development of homometallic clusters in the aspect of structural varieties.

In contrast, the intramolecular π-aromatization can enhance the stability of planar organic compounds having various structural features, accompanying the polarization of C–C π-bonds over a conjugated system in organic chemistry. Examples of such compounds include methylenecyclopropane (**I**),[9] fulvene (**II**),[10] calicene (**III**),[11] and azulene (**IV**)[12] (Figure 1a), which would undergo intramolecular π-aromatization, giving rise to more stable aromatic zwitterionic Lewis structures.[13] This behavior has seldom been reported in metal clusters. As aromaticity can significantly contribute to the stability and reactivity control of homometallic clusters,[14] we naturally assumed that intramolecular aromatization will also carve out a place in constructing unprecedented homometallic clusters.

Based on these considerations and our previous work,[5] we herein designed and synthesize $[Au(\mu_2\text{-}ER_2)]_3$–$AuPMe_3$ clusters. The *cyclic*-$[Au(\mu_2\text{-}ER_2)]_3$ moiety contributes nine in-plane electrons (three 6s Au electrons and six in-plane electrons from the three μ_2-ER_2 bridging units), whereas the *exo*-$AuPMe_3$ moiety provides another electron. This enables intramolecular σ-aromatization to occur in the plane accompanying the formation of a highly polarized *exo*-Au–Au σ bond toward the *cyclic*-$[Au(\mu_2\text{-}ER_2)]_3$ moiety, even allowing the formation of an aromatic zwitterionic Lewis structure (Figure 1b). To the best of our knowledge, the neutral Au_4 cluster has not yet been isolated in the laboratory, but theoretical chemists have predicted that it could have two possible molecular geometries: a C_{2v} Y-shape or a D_{2h} rhombus.[15] This uncertainty underscores the importance of precise synthesis of the Au_4 cluster at atomic-level, meanwhile, which is also a great challenge for synthetic chemists.[16] Here, we report the synthesis of $(R_2EAu)_3$-$AuPMe_3$ (E = Ge (**2a**), and Sn (**2b**); R_2 = 1,1,4,4-tetrakis(trimethylsilyl)butane-1,4-diyl) clusters through the rarely nucleophilic substitution reaction of $(R_2EAu)_3$ anion with Me_3PAuCl, and demonstrate that the polarity of the *exo*-Au–Au bond can be tuned by the strength of σ-aromaticity, even resulting in a distinct ionization behavior of the two clusters in solution (Figure 1b).

10.1002/anie.202311230

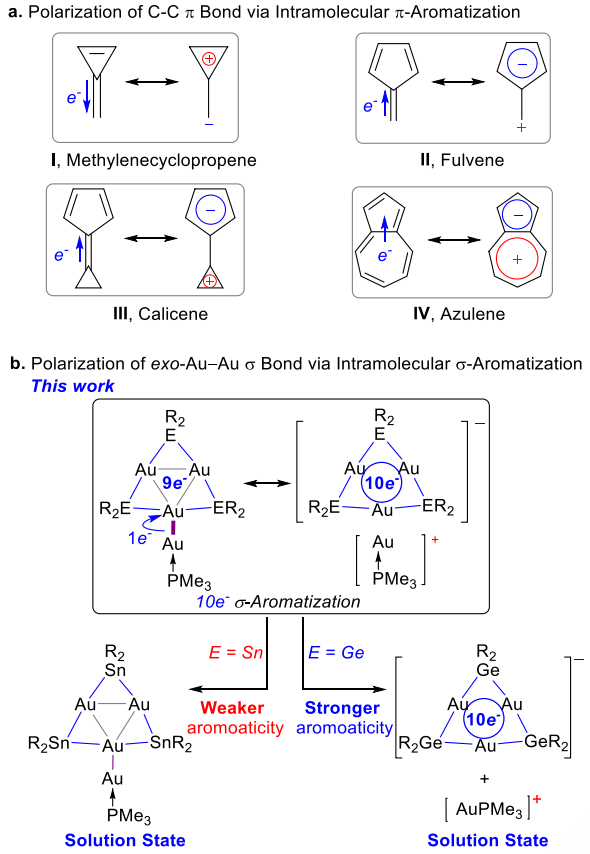

Figure 1. Molecules involving different types of intramolecular aromatization. a) Organic molecules stabilized through intramolecular π-aromatization. b) $(R_2EAu)_3$-$AuPMe_3$ stabilized through intramolecular σ-aromatization in solid state and the distinct ionization behavior of $(R_2EAu)_3$-$AuPMe_3$ in solution state tuned by σ-aromaticity.

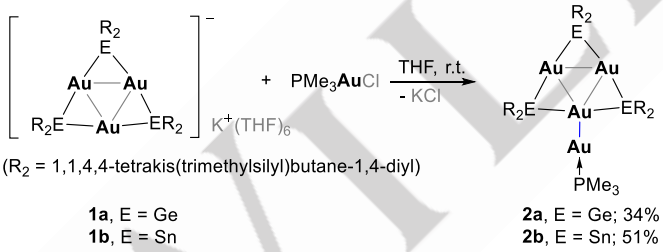

Scheme 1. Synthesis of **2a** and **2b**.

The synthesis of ligand-enveloped Au_4 clusters **2a** and **2b** was achieved through a metathesis reaction, in which an excess amount of Me_3PAuCl was added to a tetrahydrofuran (THF) solution of *cyclic*-$[Au(\mu_2\text{-}ER_2)]_3K$ (**1a** and **1b**)[5] at room temperature to yield, respectively, the tetragold(0) complexes **2a** (34%) and **2b** (51%) as green solids (Scheme 1). The tetragold(0) clusters **2a** and **2b** were stable under inert conditions and exhibited poor solubility in nonpolar hydrocarbons but decomposed in chlorinated solvents and acetonitrile. Single crystals of these complexes were obtained by volatilizing their THF solutions in a glovebox at −30 °C. The structures of **2a** and **2b** were characterized using single-crystal X-ray diffraction, multinuclear NMR spectroscopy, and high-resolution mass spectrometry. The experimental details are provided in the Supporting Information (SI).

Single-crystal X-ray diffraction analysis revealed that both molecular structures **2a** and **2b** in the solid state exhibited nearly reflectional symmetry, with the *exo*-Au atom located almost on the reflection symmetry plane (Figure 2).[17] The Au2–Au3 bond adopted a coplanar configuration with a *cyclic*-Au_3 ring in both structures. The Ge1–Au2 bond length in **2a** (2.5334(9) Å) was considerably longer than that for Ge1–Au1 (2.4807(9) Å) and known Ge–Au bond lengths (2.3271−2.4277 Å).[18] On the other hand, the Au1–Au4 bond length in **2a** (2.7188(6) Å) was significantly shorter than those of Au1–Au2 (2.8471(5) Å) and **1a** (average 2.8498 Å), where the shortest Au–Au distance was 2.5932(6) Å, which was assigned to the Au2–Au3 bond. In contrast to the structural parameters of **2a**, the three Ge–Au bonds in **1a** (average 2.4780 Å) were almost equal.[5a] In **2b**, the intraannular Au–Au bond distances were slightly longer than those in **2a**; however, the exocyclic Au2–Au3 bond length was 0.02 Å shorter. The three intraannular gold atoms remained in an isosceles triangular coordination environment, with the Au1–Au2–Au4 angle being 57.04° for **2a** and 57.67° for **2b**, and the Au4–Au1–Au2 angle being 61.48° for **2a** and 61.75° for **2b**. In contrast to the trigold anions **1a** and **1b**, the *cyclic*-$(R_2EAu)_3$ moiety was distorted in both **2a** and **2b**, which could be attributed to the presence of the *exo*-Au–Au bond.

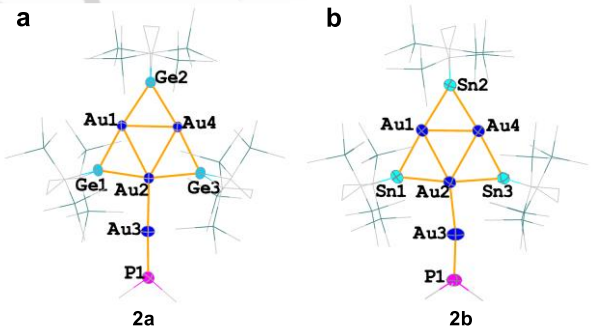

Figure 2. Molecular structures of **2a** and **2b**. Hydrogen atoms were omitted for clarity. Thermal ellipsoids are shown at the 50% probability level. Trimethylsilyl and methyl groups are depicted in a wireframe model.

In the ^{1}H NMR spectrum of **2a** at room temperature in C_6D_6, the signals of the methylene and trimethylsilyl (TMS) protons in 1,1,4,4-tetrakis(trimethylsilyl)butane-1,4-diyl appeared at 2.16 and 0.47 ppm, respectively, as sharp singlets (Figure S1), indicating that the three dialkylgermylene ligands were equivalent in solution. However, the solid structure shows that the three dialkylgermylene ligands have different chemical environments (Figure 2a). The other sharp doublet at 0.62 ppm with a coupling constant of 12 Hz was assigned to the methyl protons of PMe_3. In contrast, the ^{1}H NMR spectrum of **2b** displayed broadening of the TMS proton signals at 0.19, 0.22, and 0.24 ppm, and two singlet peaks at the chemical shift at 2.75 and 2.78 ppm (intensity ratio 2:1), which were assigned to the ring methylene protons (Figure S5). In other words, unlike those in **2a**, the three dialkylstannylene ligands in **2b** were not equivalent and can be divided into two types at a ratio of 1:2. Trimethylphosphine ligated to the *exo*-Au

10.1002/anie.202311230

atom exhibited a doublet signal in the ^{1}H NMR at 1.69 ppm with a coupling constant of 12 Hz and a signal in the ^{31}P NMR at 7.71 ppm (Figure S8). The ^{13}C and ^{29}Si spectra of **2b** at room temperature were also consistent with those of the solid structures determined by X-ray crystallography (Figure 2b).

To obtain a concise and deep insight into the structure and bonding of these clusters, we first performed the geometry optimizations of **2a** and **2b** at the PBE0-D3/def2-svp level of theory (See SI for computational details). Overall, our optimized structures closely reproduced the crystal structures, with only a minor discrepancy in the relative position between the *exo*-Au atom and the *cyclic*-$(AuGe)_3$ moiety for **2a** (see Figure S25 and accompanying remarks for a detailed comparison and explanation). We then employed an orbital alignment procedure to construct the net skeletal bonding molecular orbitals (Skeletal MOs) for the Au–Au and Au–E bonding interactions in **2a**, which was achieved by subtracting the electron densities of Au, R_2E, and phosphine from the total density matrix of the overall clusters.[19] From this, the alignment frontier molecular orbitals (Alignment FMOs) were obtained to visualize the bonding interactions among the skeletal gold/germanium (or tin) atoms. The top row of Figure 3 shows the plots of the five alignment FMOs that accommodate the ten in-plane electrons, which demonstrate that these electrons are delocalized along the *cyclic*-$(AuE)_3$ moiety with participation of the *exo*-Au atom.

To better understand the five alignment FMOs discussed above, we presented a schematic orbital diagram in Figure S13a for the *cyclic*-$[Au(\mu_2\text{-}ER_2)]_3^-$ anion fragment, illustrating the orbital interaction between the inner Au_3 triangle and outer $(\mu_2\text{-}ER_2)_3$ triangle. Each $(\mu_2\text{-}ER_2)$ bridging unit in this diagram contributed two in-plane fragment orbitals (one sp^2 hybrid orbital and one in-pane p orbital), whereas each Au orbital contributed one 6s orbital. The resulting bonding orbitals for *cyclic*-$[Au(\mu_2\text{-}ER_2)]_3$ corresponded to *1a₁′*, *1e′*, and *2e′* Mulliken symbols. Subsequently, the orbital interactions between *cyclic*-$[Au(\mu_2\text{-}ER_2)]_3^-$ anion and the *exo*-$(AuPMe_3)^+$ cation fragments, as shown in Figure S13b, results in five skeletal bonding MOs (*1a₁*, *2a₁*, *1b₂*, *3a₁*, and *2b₂*) for the entire cluster molecule $[Au(\mu_2\text{-}ER_2)]_3$–$AuPMe_3$. Sketches of these five occupied Skeletal MOs correlated well with the above-discussed five alignment FMOs (Figure 3). Overall, these results reveal the indispensable role of the in-plane 4p(Ge)/5p(Sn) and sp^2(Ge/Sn) orbitals in the construction of ten-electron delocalization systems of Au_4 clusters.

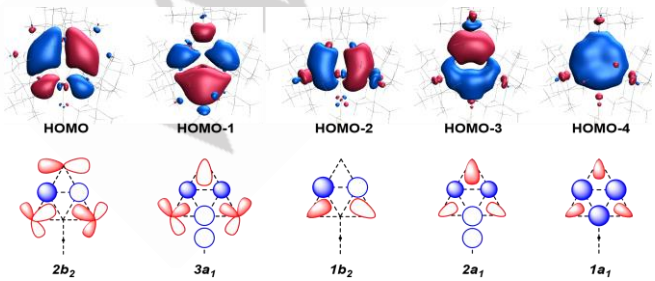

Figure 3. The five occupied Alignment FMOs (top row) and the corresponding schematic Skeletal MOs (bottom row) for **2a** that accommodate the ten in-plane electrons in the aromatic system (isovalue = 0.05).

We then performed additional electronic structure analyses to gain further insight into the properties of the *exo*-Au–Au bond in **2a** and **2b**. The calculated Mulliken charges for **2a** and **2b** have been compared in Figure 4a, in which the *exo*-Au–Au bond in **2a** was more polar, with a more negative Mulliken charge (–2.53) on *cyclic*-$(AuGe)_3$ moiety.[20] Natural bond orbital (NBO) analysis was consistent with these results, showing that the *cyclic*-$(AuGe)_3$ moiety possessed a more negative NBO charge than the *cyclic*-$(AuSn)_3$ moiety by 0.42 e^-.[21] From the ^{1}H NMR data discussed above, we conclude that the ionization of **2a** to *cyclic*-$[R_2GeAu]_3^-$ and $[AuPMe_3]^+$ occurs in solution. This is consistent with the findings from the Mulliken charge and NBO analysis, which indicate **2a** has a highly polarized *exo*-Au–Au bond. In contrast, **2b** remains neutral in solution due to the relatively lower polarity of its *exo*-Au–Au bond (Figure 4b).

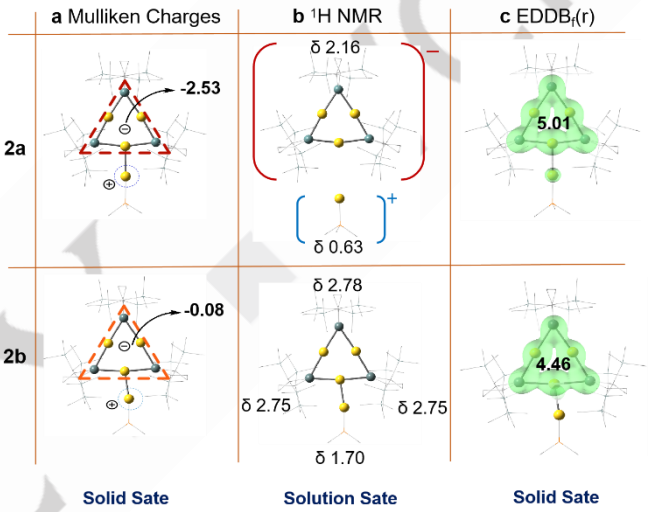

Figure 4. Polarity, ionization, and aromaticity data for **2a** and **2b**. a) Tunable polarity of the *exo*-Au-Au bond verified by Mulliken charges of *cyclic*-$(AuE)_3$ moiety and that of *exo*-Au atom. b) The distinct ionization behavior verified by the ^{1}H NMR data for ring-CH_2 and $P(CH_3)_3$. c) The calculated populations (|e|) of electron density of delocalized bonds in the *cyclic*-$(AuE)_3$ moiety with $EDDB_f(r)$ contours.

The significant differences observed experimentally in ionization between **2a** and **2b** can be attributed to their varying levels of σ-aromaticity. The high-polar *exo*-Au–Au bond of **2a** and **2b** allowed electron transfer from the *exo*-Au atom to the *cyclic*-$(AuE)_3$ moiety, leading to intramolecular σ-aromatization. Nucleus-independent chemical shift (NICS) calculations were performed to verify the intramolecular σ-aromatization of **2a** and **2b**.[22] The NICS(0) and NICS(1) values at the center of *cyclic*-$(AuGe)_3$ moiety for **2a** were calculated to be –22.97 and –12.74 ppm, those for **2b** were –21.52 and –12.41 ppm, respectively. **2a**, therefore, has a stronger σ-aromaticity in its *cyclic*-$(R_2GeAu)_3$ moiety, resulting in a greater degree of *exo*-Au–Au bond polarization and even plausible ionization in solution.

Since the magnetically induced local paratropic current on the Au atoms could potentially taint the NICS values and the core-electron contributions to the molecular magnetic response might contaminate the NICS values as well,[23] to precisely determine the relative aromaticity and identify the intrinsic reasons for tunability of the polarity of the *exo*-Au–Au bond, the electron

10.1002/anie.202311230

density of the delocalized bonds (EDDB) was calculated.[24] **2a** has an $EDDB_f(r)$ at 5.01e in the *cyclic*-$(AuGe)_3$ moiety, while **2b** cluster possesses an $EDDB_f(r)$ at 4.46e in the *cyclic*-$(AuSn)_3$ moiety (Figure 4c). These quantitative results indicate that the strength of the aromaticity in **2a** is approximately 12% greater than that in **2b**, which represents a stronger intramolecular σ-aromatization and results in a higher polarity of *exo*-Au–Au bond in **2a**. For comparison, the $EDDB_f(r)$ of **1a** was also calculated to be 6.07e (Table S2). This value is comparable to that of **2a**, confirming that cyclic-$[Au(\mu_2\text{-}ER_2)]_3^-[Au(PMe_3)]^+$ is a more efficient form for electron delocalization.

To get closer to the truth of electron delocalization and aromaticity, we conducted further analyses on the simplified *cyclic*-$[Au(EH_2)]_3^-$ (**2a′**, E = Ge; **2b′**, E = Sn) anion fragments. Figure 5a shows the gauge-including magnetically induced current (GIMIC) density[25] of the *cyclic*-$[Au(GeH_2)]_3^-$ anion fragment (**2a′**), which revealed the presence of a magnetically induced ring current. Figure 5b is the corresponding modulus density plot showing the presence of a local paratropic current (indicated in red) on the Ge and Au atoms and a diatropic ring current (marked in yellow) along the *cyclic*-$(AuGe)_3$ moiety (See the GIMIC plots of **2b′**, benzene, and H_3^+ in Figures S14-18). To quantify the strength of the ring currents in **2a′** and **2b′**, two integration planes were investigated including plane-1 and plane-2 (Figure S19 shows the integration planes). As depicted in Figure 5b, strong local paratropic currents on the Au atoms can significantly affect the integral current densities calculated on plane-1, leading to inaccurate values. In contrast, the influence of these local currents on the values obtained from integration plane-2 was negligible. Thus, the net ring current densities obtained for plane-2 are at +14.2 nA/T in **2a′** and +14.1 nA/T in **2b′**, further supporting the stronger aromaticity in **2a′**. For comparison, the induced ring density of benzene was +12.2 nA/T, whereas that of H_3^+ was +4.5 nA/T (Figures S20 and S21 show the corresponding integration planes).

Natural resonance theory (NRT),[26] and block-localized wavefunction analyses (BLW)[27] were also conducted to verify primary resonance mode of the *cyclic*-$[Au(EH_2)]_3^-$ anion fragment (**2a′** and **2b′**) and extra cyclic resonance energy (62.9 kcal/mol for **2a′** and 57.8 kcal/mol for **2b′**), which further confirmed the aromaticity within the *cyclic*-$(AuE)_3$ moiety and the relatively higher level of aromaticity in **2a′**. (Figure S22 and Figure S23) These results further prove that aromatic zwitterionic Lewis structures, *cyclic*-$[Au(\mu_2\text{-}ER_2)]_3^-[Au(PMe_3)]^+$, are more stable than their non-polarized Lewis structures.

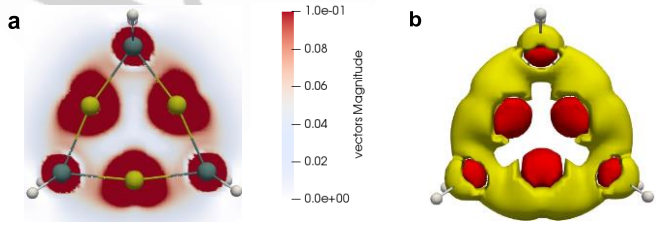

Figure 5. GIMIC plots for the *cyclic*-$[Au(GeH_2)]_3^-$ anion fragment. a) Vector magnitude plots of magnetically induced current density on the *cyclic*-$(AuGe)_3$ plane. b) Modulus density plots of the magnetically induced current in the *cyclic*-$[Au(GeH_2)]_3^-$ anion fragment (isovalue = ± 0.05). The yellow parts represent diatropic ring currents and the red parts represent local paratropic currents.

In conclusion, we have demonstrated an unprecedented nucleophilic substitution reaction of Au_3 anionic building block with PMe_3AuCl resulting in the precise synthesis of ligand-enveloped Au_4 clusters, where the isolable and non-highly symmetric homometallic clusters **2a** and **2b** possessing *exo*-gold tails have been successfully synthesized at ambient conditions. Moreover, by referring to the commonly intramolecular π-aromatization in organic chemistry, we introduce a novel stabilization mode, intramolecular σ-aromatization, which facilitates the construction of metal clusters with unusual topologies and helps construct the high-polar *exo*-metal-metal bond. Notably, the polarity of the *exo*-Au–Au bonds can be tuned via the strength of σ-aromaticity. Consequently, cluster **2a** exhibits abnormal ionization behavior of the *exo*-Au–Au bond in solution due to its stronger σ-aromaticity. Overall, the Au_3 anionic cluster acts as a building block for the construction of novel oligomeric gold(0) clusters, thus unveiling new reactivity and electronic properties of these species which are currently under active investigation in our laboratory.

Acknowledgements

This work was financially supported by the National Natural Science Foundation of China (Grant No. 22101068 and 22071039), the Natural Science Foundation of Zhejiang Province (Grant No. LQ21B020007) and the Research Grants Council of Hong Kong (HKUST 16302222). The theoretical work was supported by Shanxi Supercomputing Centre of China, and the calculations were performed on TianHe-2. We are extremely grateful to Professor Dariusz W. Szczepanik of Jagiellonian University, Professor Xuhui Lin of Central South University, Professor Jun Zhu of The Chinese University of HongKong, Shenzhen, and Mr. Shaogeng Zeng of Zhejiang Unviversity for their valuable discussion in this work.

Conflict of interest

Authors declare no competing interests.

Data Availability Statement

The data that support the findings of this study are available in the Supporting material of this article.

Keywords: metal-metal bond • electronic structure • homometallic clusters • intramolecular σ-aromatization • gold clusters

[1] a) M. Faraday, *Philos. Trans. R. Soc. London,* **1825**, *115*, 440–446; b) A. W. Hofmann, *Proc. R. Soc. London* **1856**, *8*, 1–3.
[2] a) M. Solà, A. I. Boldyrev, M. K. Cyrański, T. M. Krygowski, G. Merino, *Aromaticity and Antiaromaticity: Concepts and Applications*, Wiley, **2022**; b) G. Merino, M. Solà, I. Fernández, C. Foroutan-Nejad, P. Lazzeretti, G. Frenking, H. L. Anderson, D. Sundholm, F. P. Cossío, M. A. Petrukhina, J. Wu, J. I. Wu, A. Restrepo, *Chem. Sci.* **2023**, *14*, 5569-5576.
[3] a) A. E. Kuznetsov, K. A. Birch, A. I. Boldyrev, X. Li, H.-J. Zhai, L.-S. Wang, *Science* **2003**, *300*, 622-625. b) R. Islas, T. Heine, G. Merino, *J. Chem. Theory Comput.* **2007**, *3*, 775-781.
[4] a) T. J. Robilotto, J. Bacsa, T. G. Gray, J. P. Sadighi, *Angew. Chem. Int. Ed.* **2012**, *51*, 12077-12080; b) L. Jin, D. S. Weinberger, M. Melaimi, C. E. Moore, A. L. Rheingold, G. Bertrand, *Angew. Chem.* **2014**, *126*, 9205-9209.
[5] a) Y. Li, G. Zhen, L. Huang, R. Zhang, L. Wang, F. Qi, M. Kira, Z. Li, *Chem. Commun.* **2022**, *58*, 6705-6708; b) L. Wang, J. Xu, M. Kira, L. Yan, X.-Q. Xiao, Z. Li, *Angew. Chem. Int. Ed.* **2020**, *59*, 1980-1984.

[6] K. Freitag, C. Gemel, P. Jerabek, I. M. Oppel, R. W. Seidel, G. Frenking, H. Banh, K. Dilchert, R. A. Fischer, *Angew. Chem. Int. Ed.* **2015**, *54*, 4370-4374.
[7] H.-J. Zhai, B. B. Averkiev, D. Y. Zubarev, L.-S. Wang, A. I. Boldyrev, *Angew. Chem. Int. Ed.* **2007**, *46*, 4277-4280.
[8] a) J. T. Boronski, J. A. Seed, D. Hunger, A. W. Woodward, J. van Slageren, A. J. Wooles, L. S. Natrajan, N. Kaltsoyannis, S. T. Liddle, *Nature* **2021**, *598*, 72-75; b) X. Lin, Y. Mo, *Angew. Chem. Int. Ed.* **2022**, *61*, e202209658.
[9] T. D. Norden, S. W. Staley, W. H. Taylor, M. D. Harmony, *J. Am. Chem. Soc.* **1986**, *108*, 7912-7918.
[10] a) T. M. Krygowski, W. P. Oziminski, M. Palusiak, P. W. Fowler, A. D. McKenzie, *Phys. Chem. Chem. Phys.* **2010**, *12*, 10740-10745; b) P. Preethalayam, K. S. Krishnan, S. Thulasi, S. S. Chand, J. Joseph, V. Nair, F. Jaroschik, K. V. Radhakrishnan, *Chem. Rev.* **2017**, *117*, 3930-3989.
[11] B. A. Shainyan, A. Fettke, E. Kleinpeter, *J. Phys. Chem. A* **2008**, *112*, 10895-10903.
[12] H. Möllerstedt, M. C. Piqueras, R. Crespo, H. Ottosson, *J. Am. Chem. Soc.* **2004**, *126*, 13938-13939.
[13] B. A. Hess, Jr., L. J. Schaad, *J. Am. Chem. Soc.* **1971**, *93*, 305-310.
[14] a) M. Solà, *Nat. Chem.* **2022**, *14*, 585-590; b) X.-W. Li, W. T. Pennington, G. H. Robinson, *J. Am. Chem. Soc.* **1995**, *117*, 7578-7579.
[15] a) G. Zanti, D. Peeters, in *Theoretical Chemistry in Belgium: A Topical Collection from Theoretical Chemistry Accounts* (Eds.: B. Champagne, M. S. Deleuze, F. De Proft, T. Leyssens), Springer Berlin Heidelberg, Berlin, Heidelberg, **2014**, pp. 261-275; b) Y. Li, V. Oliveira, C. Tang, D. Cremer, C. Liu, J. Ma, *Inorg. Chem.* **2017**, *56*, 5793-5803; c) L. Xiao, B. Tollberg, X. Hu, L. Wang, *J. Chem. Phys.* **2006**, *124*, 114309; d) B. Assadollahzadeh, P. Schwerdtfeger, *J. Chem. Phys.* **2009**, *131*, 064306.
[16] a) A. Li, Z. Tan, Y. Hu, Z. Lu, J. Yuan, X. Li, J. Xie, J. Zhang, K. Zhu, *J. Am. Chem. Soc.* **2022**, *144*, 2085-2089; b) L. Xing, Z. Peng, W. Li, K. Wu, *Acc. Chem. Res.* **2019**, *52*, 1048-1058; c) N. G. Engelis, A. Anastasaki, G. Nurumbetov, N. P. Truong, V. Nikolaou, A. Shegiwal, M. R. Whittaker, T. P. Davis, D. M. Haddleton, *Nat. Chem.* **2017**, *9*, 171-178; d) Q. Zhou, K. Song, G. Zhang, X. Song, J. Lin, Y. Zang, D. Zhang, D. Zhu, *Nat. Commun.* **2022**, *13*, 1803; e) A. Dasgupta, H. He, R. Gong, S.-L. Shang, E. K. Zimmerer, R. J. Meyer, Z.-K. Liu, M. J. Janik, R. M. Rioux, *Nat. Chem.* **2022**, *14*, 523-529; f) Y. Kohsaka, K. Nakazono, Y. Koyama, S. Asai, T. Takata, *Angew. Chem. Int. Ed.* **2011**, *50*, 4872-4875; g) A.-M. L. Fuller, D. A. Leigh, P. J. Lusby, *Angew. Chem. Int. Ed.* **2007**, *46*, 5015-5019; h) R. P. Herrera, M. C. Gimeno, *Chem. Rev.* **2021**, *121*, 8311-8363; i) J. Zheng, Z. Lu, K. Wu, G.-H. Ning, D. Li, *Chem. Rev.* **2020**, *120*, 9675-9742; j) H. Qian, M. Zhu, Z. Wu, R. Jin, *Acc. Chem. Res.* **2012**, *45*, 1470-1479; k) Y. Du, H. Sheng, D. Astruc, M. Zhu, *Chem. Rev.* **2020**, *120*, 526-622; l) S.-T. Tung, C.-C. Lai, Y.-H. Liu, S.-M. Peng, S.-H. Chiu, *Angew. Chem. Int. Ed.* **2013**, *52*, 13269-13272; m) A.-M. L. Fuller, D. A. Leigh, P. J. Lusby, A. M. Z. Slawin, D. B. Walker, *J. Am. Chem. Soc.* **2005**, *127*, 12612-12619; n) J. D. Megiatto, Jr., D. I. Schuster, *J. Am. Chem. Soc.* **2008**, *130*, 12872-12873; o) P. R. Ashton, T. T. Goodnow, A. E. Kaifer, M. V. Reddington, A. M. Z. Slawin, N. Spencer, J. F. Stoddart, C. Vicent, D. J. Williams, *Angew. Chem. Int. Ed. Engl.* **1989**, *28*, 1396-1399; p) D. G. Hamilton, J. K. M. Sanders, J. E. Davies, W. Clegg, S. J. Teat, *Chem. Commun.* **1997**, 897-898; q) P. Cui, H.-S. Hu, B. Zhao, J. T. Miller, P. Cheng, J. Li, *Nat. Commun.* **2015**, *6*, 6331.
[17] Deposition numbers 2222847 (for **2a**), and 2222848 (for **2b**) contain the supplementary crystallographic data for this paper. These data are provided free of charge by the joint Cambridge Crystallographic Data Centre and Fachinformationszentrum Karlsruhe Access Structures service..
[18] a) D. Matioszek, T.-G. Kocsor, A. Castel, G. Nemes, J. Escudie, N. Saffon, *Chem. Commun.* **2012**, *48*, 3629-3631; b) A. Bauer, H. Schmidbaur, *J. Am. Chem. Soc.* **1996**, *118*, 5324-5325; c) J. Hlina, H. Arp, M. Walewska, U. Flörke, K. Zangger, C. Marschner, J. Baumgartner, *Organometallics* **2014**, *33*, 7069-7077; d) Z. Dong, K. Bedbur, M. Schmidtmann, T. Müller, *J. Am. Chem. Soc.* **2018**, *140*, 3052-3060; e) L. Álvarez-Rodríguez, J. A. Cabeza, P. García-Álvarez, D. Polo, *Organometallics* **2015**, *34*, 5479-5484.
[19] J.-X. Zhang, F. K. Sheong, Z. Lin, *Inorg. Chem.* **2020**, *59*, 8864-8870.
[20] R. S. Mulliken, *J. Chem. Phys.* **1955**, *23*, 1833-1840.
[21] E. D. Glendening, C. R. Landis, F. Weinhold, *J. Comput. Chem.* **2013**, *34*, 1429-1437.
[22] Z. Chen, C. S. Wannere, C. Corminboeuf, R. Puchta, P. v. R. Schleyer, *Chem. Rev.* **2005**, *105*, 3842-3888.
[23] a) B. J. R. Cuyacot, C. Foroutan-Nejad, *Nature* **2022**, *603*, E18-E20; b) C. Foroutan-Nejad, J. Vícha, A. Ghosh, *Phys. Chem. Chem. Phys.* **2020**, *22*, 10863-10869. c) M. Orozco-Ic, N. D. Charistos, A. Muñoz-Castro, R. Islas, D. Sundholm, G. Merino, *Phys. Chem. Chem. Phys.* **2022**, *24*, 12158-12166.
[24] D. W. Szczepanik, M. Andrzejak, J. Dominikowska, B. Pawełek, T. M. Krygowski, H. Szatylowicz, M. Solà, *Phys. Chem. Chem. Phys.* **2017**, *19*, 28970-28981.
[25] a) J. Jusélius, D. Sundholm, J. Gauss, *J. Chem. Phys.* **2004**, *121*, 3952-3963; b) H. Fliegl, S. Taubert, O. Lehtonen, D. Sundholm, *Phys. Chem. Chem. Phys.* **2011**, *13*, 20500-20518.
[26] a) E. D. Glendening, F. Weinhold, *J. Comput. Chem.* **1998**, *19*, 593-609; b) E. D. Glendening, F. Weinhold, *J. Comput. Chem.* **1998**, *19*, 610-627; c) E. D. Glendening, J. K. Badenhoop, F. Weinhold, *J. Comput. Chem.* **1998**, *19*, 628-646.
[27] Y. Mo, L. Song, Y. Lin, *J. Phys. Chem. A* **2007**, *111*, 8291-8301.

10.1002/anie.202311230

WILEY VCH

COMMUNICATION

Entry for the Table of Contents

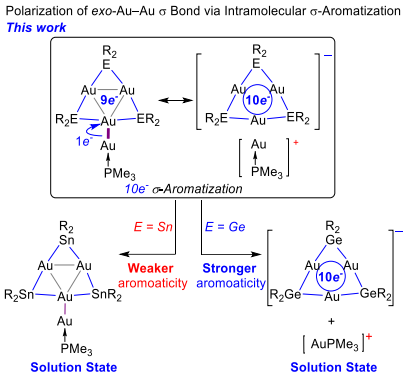

Ligand-enveloped tetragold(0) clusters have been successfully synthesized via a nucleophilic substitution reaction between a Au_3 anionic cluster and PMe_3AuCl. A novel stabilization mode, intramolecular σ-aromatization has been discovered, in which the intramolecular σ-aromatization has now been observed for the first time in homometallic clusters, and the polarity of the *exo*-Au-Au bonds can be tuned via the strength of σ-aromaticity.